

Continuous Reset Element:

Transient and Steady-state Analysis for Precision Motion Systems

Nima Karbasizadeh, S. Hassan HosseinNia¹

*Department of Precision and Microsystem Engineering, Delft University of Technology,
Delft, The Netherlands*

Abstract

This paper addresses the main goal of using reset control in precision motion control systems, breaking of the well-known “Waterbed effect”. A new architecture for reset elements will be introduced which has a continuous output signal as opposed to conventional reset elements. A steady-state precision study is presented, showing the steady-state precision is preserved while the peak of sensitivity is reduced. The architecture is then used for a “Constant in Gain Lead in Phase” (CgLp) element and a numerical analysis on transient response shows a significant improvement in transient response. It is shown that by following the presented guideline for tuning, settling time can be reduced and at the same time a no-overshoot step response can be achieved. A practical example is presented to verify the results and also to show that the proposed element can achieve a complex-order behaviour.

Keywords: Precision Motion Control, Constant in Gain Lead in Phase, Reset Control Systems, Waterbed Effect

1. Introduction

Waterbed effect limits the performance of the linear control systems [1]. Almost every researcher in the field of control engineering has encountered this fundamental limitation. One can come up with different mathematical interpretations for it, however, most definitely, its practical effect is more important,

¹Corresponding Author

especially for high-tech industrial applications such as precision motion control. One can interpret this effect by putting transient and steady-state response of the system on two sides of this infamous waterbed, which implicates that by improving one, you are sacrificing the other.

10 Reset control systems, first proposed by Clegg in [2], are proving themselves as alternatives for linear control systems as they showed potential to outperform linear control systems by breaking waterbed effect limitation. Clegg proposed an integrator whose output will reset to zero whenever its input crosses zero. It was later established that based on Describing Function (DF) analysis, such an
15 action will reduce the phase lag of the integrator by 52° . Although this already breaks the Bode's gain-phase relation for linear control systems, there are concerns while using Clegg's Integrator (CI) in practice, namely, the accuracy of DF approximation, limit-cycle, etc.

In order to address the drawbacks and exploiting the benefits, the idea was
20 later extended to more sophisticated elements such as "First-Order Reset Element" [3, 4] and "Second-Order Reset Element" [5] or using Clegg's integrator in form of PI+CI [6] or resetting the state to a fraction of its current value, known as partial resetting [7]. Reset control has also recently been used to approximate the complex-order filters [8, 9]. Advantage of using reset control over
25 linear control has been shown in many studies especially in precision motion control [10, 11, 12, 7, 13, 14, 15, 16, 17, 18]. However, these studies are mostly focused on solving one problem. For example they either improve transient [19] or steady-state response of the system while paying little or no attention to the other.

30 One of the recent studies introduces a new reset element called "Constant-in-Gain, Lead-in-Phase" (CgLp) element which is proposed based on the loop-shaping concept [9]. DF analysis of this element shows that it can provide broadband phase lead while maintaining a constant gain. Such an element is used in the literature to replace some part of the differentiation action in PID
35 controllers as it will help improve the precision of the system according to loop-shaping concept [18, 12, 13, 9].

In [12, 18], it is suggested that DF analysis for reset control systems can be inaccurate as it neglects the higher-order harmonics created in response of reset control systems. These studies also suggest that suppressing higher-order har-
40 monics can improve the steady-state precision of the system.

One of the benefits of providing phase lead through CgLp is improving the transient response properties of the system, as it is shown that it reduces the overshoot and settling time of the system. However, the way to achieve this goal is not only through phase compensation around cross-over frequency. It is shown
45 in [20] that since reset control systems are nonlinear systems, the sequence of elements in control loop affects the output of the system. It was shown that when the lead elements are placed before reset element, it can improve the overshoot of the system. However, no systematic approach is proposed there for further improving the transient response. In [21], it is shown that by changing the re-
50 setting condition of reset element to reset based on its input and its derivative, overshoot limitation in linear control, systems can be overcome. This limitation has also been broken using the same technique in another hybrid control system called “Hybrid Integrator Gain System” (HIGS) [22]. However, in these studies the effect of such an action on steady-state performance of the system is not
55 addressed.

Another important common properties of all reset elements in the literature is the discontinuity of the output signal. This properties is a cause for presence of high-frequency content in the signals and subsequent practical issues [18]. Continuous time implementation as opposed to discrete time implementation of
60 reset control and also soft resetting were introduced in the literature to mitigate this problem to some extent [23, 24]. However, this paper proposes an approach which can also used in discrete time.

The main contribution of this paper is to propose a new architecture for CgLp element which has a continuous output as opposed to conventional reset el-
65 ements. This element will drastically improves the transient response of the systems without jeopardizing the steady-state performance of the system by increasing higher-order harmonics. This paper shows that this architecture even

reduces the higher-order harmonics by smoothing the reset jumps. Reset control systems are also known for having big jumps and peaks in their control input
70 which can be a limiting factor in practical applications due to saturation. The proposed architecture will also improve this drawback. A guideline for tuning the propose architecture will also be provided.

The remainder of this paper is organized as follows: The first section will present the preliminaries of the study. The following section will present the continuous
75 reset architecture. Section 4 will study the open-loop steady-state properties of the proposed architecture. The following two sections will numerically study the closed-loop transient and steady-state characteristics of the proposed controller. Section 7, will verify the results by presenting the results of an experiment on a precision positioning system system and at last the paper concludes along with
80 some tips for ongoing works.

2. Preliminaries

This section will discuss the preliminaries of this study.

2.1. Dynamics of Precision Motion Systems

The first stage in precise control of a mechatronic system is to determine the
85 dynamics of motion. A friction-less moving mass is the most basic mechatronic system. Its motion dynamics are represented by a double integrator. A DC motor or a voice-coil actuator are examples of such systems. In practice, the masses are usually constrained by springs and there is always some amounts of damping present, which creates a mass-spring-damper dynamics. Such dy-
90 namics in frequency domain has a constant spring line and a resonance peak in addition to the negative-sloped mass line.

Most of the precision motion setups are well-designed systems which can be modeled as mass-spring-damper systems or a cascade of them [25, 26, 27, 28]. Whether they are collocated or non-collocated systems, in practice, the cross-
95 over frequency to control them is usually placed along the -2 slope mass line.

Furthermore, the presence of integrator at lower frequencies, makes the overall open-loop frequency domain characteristics of precision motion systems to closely resemble a mass system.

This paper consists of an analytical analysis on steady-state properties of such systems and a numerical analysis of transient properties. Although the analytical steady-state analysis will be carried out for general motion plants, for the transient numerical analysis for the sake of generality and simplicity, a mass plant will be assumed. However, it will be shown in experimental results that the study hold for a mass-spring-damper system with higher frequency modes.

2.2. General Reset Controller

The general form of reset controllers used in this study is as following:

$$\sum_R := \begin{cases} \dot{x}_r(t) = A_r x_r(t) + B_r e(t), & \text{if } e(t) \neq 0 \\ x_r(t^+) = A_\rho x_r(t), & \text{if } e(t) = 0 \\ u(t) = C_r x_r(t) + D_r e(t) \end{cases} \quad (1)$$

where A_r, B_r, C_r, D_r denote the state space matrices of the Base Linear System (BLS) and reset matrix is denoted by $A_\rho = \text{diag}(\gamma_1, \dots, \gamma_n)$ which contains the reset coefficients for each state. $e(t)$ and $u(t)$ represent the input and output for the reset controller, respectively.

A special type of reset elements which is of concern in this paper is First Order Reset Element (FORE). In the literature, this element is typically shown as $\frac{1}{s/\omega_r + 1}$, where ω_r is the corner frequency and the arrow indicates the resetting action and since element has only one resetting state, $A_\rho = \gamma$.

2.3. H_β condition

Among different criteria for stability of reset control systems [11, 29, 30, 31, 32, 33], despite of its conservativity, H_β condition has gained attention because of simplicity and frequency domain applicability [7]. In [34], the H_β condition has been reformulated such that the frequency response functions of the controllers and the plant can be used directly. This method especially includes the case

120 where the reset element is not the first element in the loop.

Theorem 1. *Let us denote frequency response functions of the open-loop BLS and the reset element as $O(j\omega)$ and $C_R(j\omega)$, respectively. And let the vector $\vec{\mathcal{N}}(\omega) \in \mathbb{R}^2$ be defined as $\vec{\mathcal{N}}(\omega) = [\mathcal{N}_X \quad \mathcal{N}_Y]^T$ in which*

$$\begin{aligned} \mathcal{N}_X &= \Re(O(j\omega)\kappa(j\omega)), \\ \mathcal{N}_Y &= \Re(\kappa(j\omega)C_R(j\omega)), \end{aligned} \tag{2}$$

where $\kappa(j\omega) = 1 + O^*(j\omega)$, $O^*(j\omega)$ is the conjugate of $O(j\omega)$ and $\Re(\cdot)$ stands for the real part of a complex number. Let

$$\theta_1 = \min_{\omega \in \mathbb{R}^+} \angle \vec{\mathcal{N}}(\omega) \text{ and } \theta_2 = \max_{\omega \in \mathbb{R}^+} \angle \vec{\mathcal{N}}(\omega). \tag{3}$$

Then the h_β condition for a reset control system is satisfied and its response is Uniformly Bounded-Input Bounded-State (UBIBS) stable if

$$\left(-\frac{\pi}{2} < \theta_1 < \pi\right) \wedge \left(-\frac{\pi}{2} < \theta_2 < \pi\right) \wedge (\theta_2 - \theta_1 < \pi). \tag{4}$$

2.4. Describing Functions

Describing function analysis is the known approach in literature for approximation of frequency response of nonlinear systems like reset controllers [35]. However, the DF method only takes the first harmonic of Fourier series decomposition of the output into account and neglects the effects of the higher order harmonics. This simplification can be significantly inaccurate under certain circumstances [12]. The ‘‘Higher Order Sinusoidal Input Describing Function’’ (HOSIDF) method has been introduced in [36] to provide more accurate information about the frequency response of nonlinear systems by investigation of higher-order harmonics of the Fourier series decomposition. In other words, in this method, the nonlinear element will be replaced by a virtual harmonic generator. This method was developed in [37] for reset elements defined by Eq. (1)

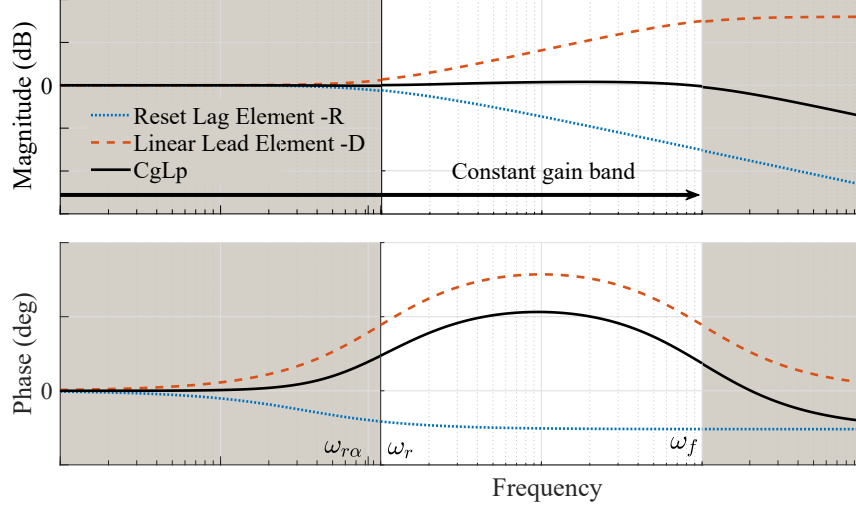


Figure 1: The concept of using combination of a reset lag and a linear lead element to form a CgLp element. The figure is from [9].

as follows:

$$\begin{aligned}
 H_n(\omega) &= \begin{cases} C_r(j\omega I - A_r)^{-1}(I + j\Theta(\omega))B_r + D_r, & n = 1 \\ C_r(j\omega n I - A_r)^{-1}j\Theta(\omega)B_r, & \text{odd } n > 1 \\ 0, & \text{even } n \geq 2 \end{cases} \\
 \Theta(\omega) &= -\frac{2\omega^2}{\pi}\Delta(\omega)[\Gamma(\omega) - \Lambda^{-1}(\omega)] \\
 \Lambda(\omega) &= \omega^2 I + A_r^2 \\
 \Delta(\omega) &= I + e^{\frac{\pi}{\omega}A_r} \\
 \Delta_\rho(\omega) &= I + A_\rho e^{\frac{\pi}{\omega}A_r} \\
 \Gamma(\omega) &= \Delta_\rho^{-1}(\omega)A_\rho\Delta(\omega)\Lambda^{-1}(\omega)
 \end{aligned} \tag{5}$$

where $H_n(\omega)$ is the n^{th} harmonic describing function for sinusoidal input with frequency of ω .

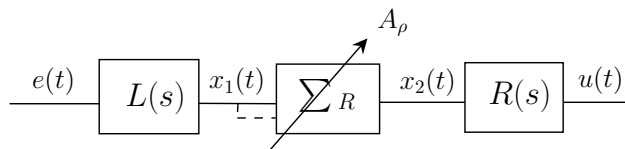


Figure 2: Proposed architecture for reset elements which includes a lead element, $L(s)$ before the reset element and its inverse after the reset element. The proposed lead is $L(s) = \frac{s/\omega_l+1}{s/\omega_h+1}$ and $R(s) = \frac{1}{s/\omega_l+1}$.

2.5. CgLp

CgLp is a broadband phase compensation reset element which has a first harmonic constant gain behaviour while providing a phase lead [9]. This element consists in a reset lag element in series with a linear lead filter, namely \sum_R and D , respectively. For FORE CgLp:

$$\sum_R = \frac{1}{s/\omega_r + 1}, \quad D(s) = \frac{s/\omega_{r\alpha} + 1}{s/\omega_f + 1} \quad (6)$$

where $\omega_{r\alpha} = \alpha\omega_r$, α is a tuning parameter accounting for a shift in corner frequency of the filter due to resetting action, and $[\omega_r, \omega_f]$ is the frequency range where the CgLp will provide the required phase lead. The arrow indicates the resetting action as described in Eq. (1).

130

CgLp provides the phase lead by using the reduced phase lag of reset lag element in combination with a corresponding lead element to create broadband phase lead. Ideally, the gain of the reset lag element should be canceled out by the gain of the corresponding linear lead element, which creates a constant gain behavior. The concept is depicted in Fig. 1.

135

3. Proposed Architecture for Continuous Reset (CR) Elements

The new architecture which this paper proposes consists of adding a first-order lag element, $R(s)$, after the reset element and adding the inverse of it, which is basically a lead element, after the reset element. Fig. 2 depicts the new

architecture in which

$$L(s) = \frac{s/\omega_l + 1}{s/\omega_h + 1}, \quad R(s) = \frac{1}{s/\omega_l + 1}. \quad (7)$$

In the ideal case, $L(s) = R^{-1}(s)$, however, in order to make $L(s)$ proper and realizable, the presence of the denominator in $L(s)$ is necessary. Nevertheless, assuming ω_h is large enough, $R(s) \approx L^{-1}(s)$ in low frequencies. In the context of linear control systems, adding these two elements would almost have no effect on the output of the system in lower frequencies and improve the noise attenuation behaviour at higher frequencies, provided the internal states stability. However, in the context of nonlinear control systems, the output of the system will be changed significantly.

In this new architecture the resetting condition is changed from $e(t) = 0$ to $x_1(t) = 0$. Again considering that ω_h is large enough, the new resetting condition can be approximated as

$$x_1(t) = \dot{e}(t)/\omega_l + e(t) = 0. \quad (8)$$

The new reset element resets based on a linear combination of $e(t)$ and $\dot{e}(t)$, where ω_l determines the weight of each. In closed loop, $e(t)$ and $\dot{e}(t)$ are the error and its differentiation.

Remark 1. According to Theorem 1, a reset element in CR architecture has the same stability properties as standing alone, as long as $O(s)$ stays the same, i.e., $R(s)$ and $L(s)$ cancel each other in linear domain. In other words, adding $L(s)$ and $R(s)$ in CR architecture, does not affect the stability properties of the reset control system. However, for the architecture presented in this paper, the additional condition is $\omega_h \gg \omega_r$ and $\omega_h \gg \omega_c$, where ω_c is the cross-over frequency.

Theorem 2. The output of the proposed architecture is continuous as opposed to \sum_R alone.

Proof. If the reset instants are $\{t_k \mid k = 1, 2, 3, \dots\}$, from Eq. (1) and Fig. 2, it can be seen that

$$\sum_R := \begin{cases} \dot{x}_r(t) = A_r x_r(t) + B_r x_1(t), & \text{if } t \neq t_k \\ x_r(t^+) = A_\rho x_r(t), & \text{if } t = t_k \\ x_2(t) = C_r x_r(t) + D_r x_1(t) \end{cases} \quad (9)$$

It is readily obvious that $x_2(t)$ is continuous on (t_{k-1}, t_k) and (t_k, t_{k+1}) . However,

$$\lim_{t \rightarrow t_k^-} x_2(t) \neq \lim_{t \rightarrow t_k^+} x_2(t) \quad (10)$$

and thus it is discontinuous. Nevertheless, for $u(t)$ one can write

$$u(t) = \omega_l \left(e^{-\omega_l(t-t_{k-1})} u(t_{k-1}) + \int_{t_{k-1}}^t e^{-\omega_l(t-\tau)} x_2(\tau) d\tau \right). \quad (11)$$

It can be readily seen that

$$\lim_{t \rightarrow t_k^-} u(t) = \lim_{t \rightarrow t_k^+} u(t) = \omega_d \left(e^{-\omega_l(t_k-t_{k-1})} u(t_{k-1}) + \int_{t_{k-1}}^{t_k} e^{-\omega_l(t_k-\tau)} x_2(\tau) d\tau \right). \quad (12)$$

□

In addition to making the reset element output continuous, other motivations to use this architecture can be described in terms of steady-state and transient response of system, which will be discussed in details in following sections.

155 4. Open-Loop Steady-State Properties of the CR Architecture

Frequency domain analysis is the popular approach for study of the steady-state response of a system. However, as mentioned earlier, because of the non-linearity of reset elements, that is not directly possible. The DF and HOSIDF methods are two approaches to approximate a frequency response for a reset control systems, where DF can be regarded as a special case of HOSIDF in

160

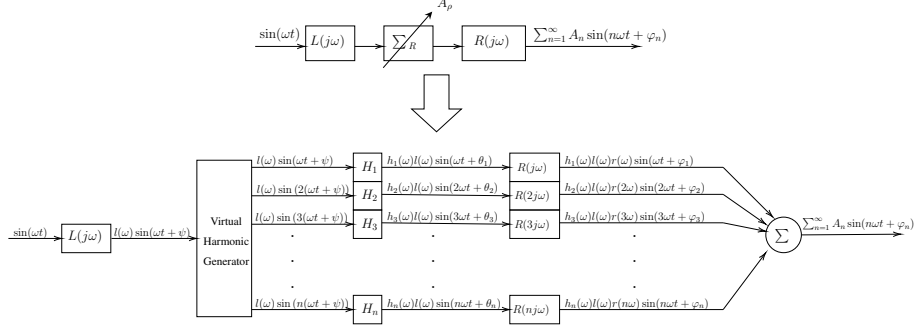


Figure 3: Representation of HOSIDF for open-loop analysis of the new architecture proposed. $l(\omega) = |L(j\omega)|$, $r(\omega) = |R(j\omega)|$ and $h_n(\omega) = |H_n(j\omega)|$, where $H_n(\omega)$ can be obtained from Eq. (5) for \sum_R .

which, only the first-order harmonic is studied. In order to illustrate how the HOSIDF approach can be used for the CR architecture proposed, one can refer to Fig. 3.

165 **Proposition 1.** For $\omega_h = \infty$, the CR architecture has the same DF as the \sum_R alone.

Proof. Let the states in CR architecture be denoted as shown in Fig. 2. For the purpose of DF and HOSIDF analysis, one should have $e(t) = \sin(\omega t)$. Obviously, the steady-state response of $x_1(t)$ is:

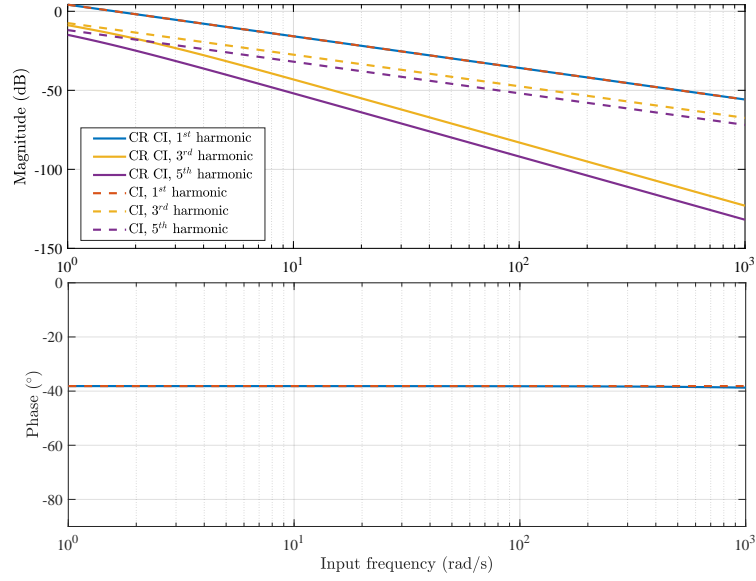
$$x_1(t) = l(\omega) \sin(\omega t + \psi(\omega)) \quad (13)$$

where $l(\omega) = |L(j\omega)|$ and $\psi(\omega) = \angle L(j\omega)$. Considering $x_1(t)$ as the input to the reset element and according to Eq. (5),

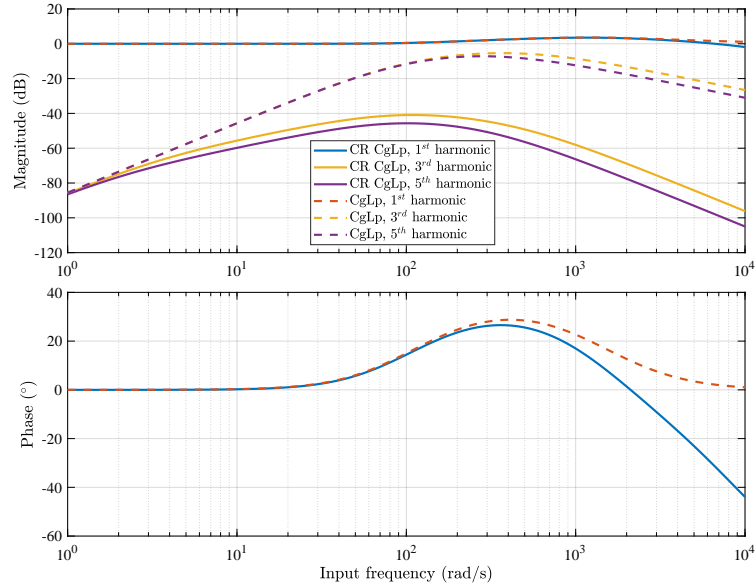
$$x_{21}(t) = h_1(\omega) l(\omega) \sin(\omega t + \theta_1(\omega)) \quad (14)$$

where $x_{21}(t)$ stands for first harmonic of $x_2(t)$ and $h_1(\omega) = |H_1(j\omega)|$ and $\theta_1(\omega) = \psi(\omega) + \angle H_1(j\omega)$. And lastly,

$$u_1(t) = h_1(\omega) l(\omega) r(\omega) \sin(\omega t + \varphi_1(\omega)) \quad (15)$$

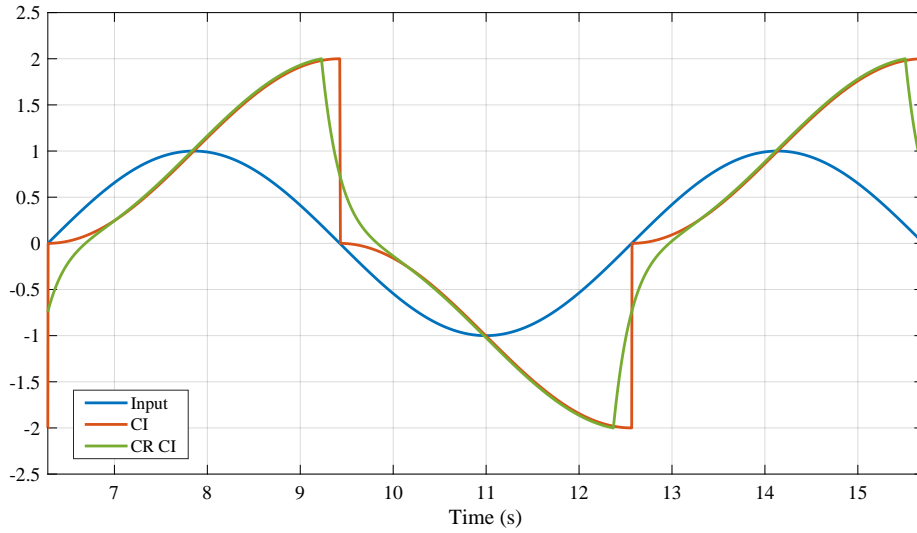


(a) HOSIDF of CI compared to CR CI. $\omega_l = 10$, $\omega_h = 1e4$ and $\gamma = 0$.

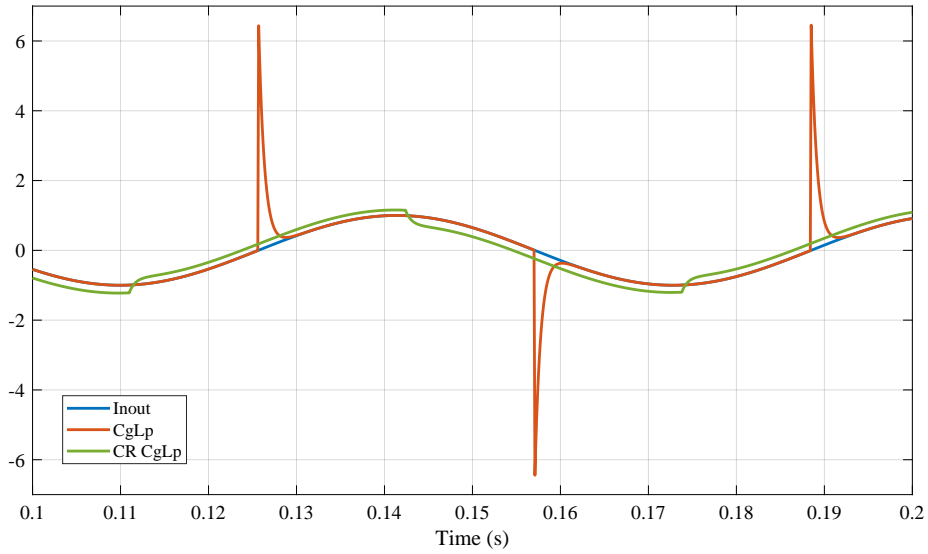


(b) HOSIDF of CgLp compared to CR CgLp. $\omega_l = 10$, $\omega_h = 1e4$, $\omega_r = 100$, $\omega_f = 1500$ and $\gamma = 0.11$.

Figure 4: HOSIDF of CI and CgLp compared to their CR architecture proposed in this paper.



(a) Sinusoidal response of Clegg Integrator (CI) compared to CR CI. Input is $\sin(t)$.



(b) Sinusoidal response of conventional CgLp compared to CR CgLp. Input is $\sin(100t)$.

Figure 5: Simulation results for sinusoidal response of CI and CgLp compared to their CR architecture proposed in this paper.

where $u_1(t)$ stands for first harmonic of $u(t)$ and $r(t) = |R(j\omega)|$ and $\varphi_1(\omega) =$

$\theta_1(\omega) + \angle R(j\omega)$. Since $R(j\omega) \approx L^{-1}(j\omega)$ for $\omega \ll \omega_h$, it can be seen that

$$|u_1(t)| = h_1(\omega), \quad (16)$$

$$\varphi_1(\omega) = \psi(\omega) + \angle H_1(j\omega) - \psi(\omega) = \angle H_1(j\omega). \quad (17)$$

□

Proposition 2. *The magnitude of higher-order harmonics for CR architecture is reduced compared to the \sum_R alone.*

Proof. Following the same reasoning as Proposition 1, one has

$$u_n(t) = h_n(\omega)l(\omega)r(n\omega) \sin(n\omega t + \varphi_n(\omega)), \quad (18)$$

where $u_n(t)$ is the n^{th} harmonic of $u(t)$, $h_n(\omega) = |H_n(j\omega)|$ and $\varphi_n = \angle H_n(j\omega) + \angle L(j\omega) + \angle R(jn\omega)$. Since $r^{-1}(\omega) \approx l(\omega)$ for $\omega_h \gg \omega_l$, and since $l(\omega)$ is an increasing function

$$A_n(\omega) < h_n(\omega), \quad (19)$$

where $A_n(\omega)$ stands for $|u_n(t)|$. In other terms, for large enough ω_h ,

$$A_n(\omega) \approx \sqrt{\frac{(\omega/\omega_l)^2 + 1}{(n\omega/\omega_l)^2 + 1}} h_n(\omega). \quad (20)$$

For $\omega \ll \omega_l$,

$$A_n(\omega) = h_n(\omega) \quad (21)$$

and for $\omega \gg \omega_l$,

$$A_n(\omega) = \frac{1}{n} h_n(\omega). \quad (22)$$

170

□

Fig. 3 illustrates the harmonic generation for CR architecture.

Theorem 2 and Propositions 1 and 2 may seem somewhat trivial, however they indicate very important features of the CR architecture in terms of steady-state performance. As mentioned earlier the frequency domain analysis and design for reset control systems heavily depends on the accuracy of DF approximation. The CR architecture maintains the DF characteristics of the reset elements and

175

reduces the higher-order harmonics which makes the DF approximation more accurate. It is shown in [12, 18] that it improves the performance of the systems in terms of steady-state precision.

180 Moreover, the discontinuity of output signal in reset controllers creates practical problems such as amplifier or actuator saturation and excitation of higher frequency modes for complex plants. The CR architecture will solve these problems by reducing the known peaks in the control input of the reset control systems. In order to illustrate the effect of the CR architecture on HOSIDF of reset elements, the HOSIDF of a Clegg Integrator (CI) and a CR CI are compared in 185 Fig. 4a, this figure shows that while the DF for these two elements are identical a significant reduction in HOSIDF of CR CI with respect to CI happens, this indicates that as we approach higher frequencies, the DF will become a more accurate approximation in CR CI. The same comparison is made for CgLp and 190 CR CgLp in Fig. 4b. Both CgLps are designed to create a phase lead of 15° at 100 rad/s while maintaining a constant gain. A significant reduction in magnitude of higher-order harmonics is also clear here, which indicates that CR CgLp has a much closer behaviour to the first-order harmonic which is the ideal behavior for reset control systems.

195 In Fig. 5, the sinusoidal response of CI vs. CR CI at 1 rad/s and CgLp vs. CR CgLp at 100 rad/s are depicted. At both comparisons, it is clear that the output of CR architecture is continuous as opposed to reset elements in their conventional form, and the response are much smoother which shows the reduction of higher-order harmonics. It has to be noted for the case of CgLp, the big peak 200 in the response, which can cause aforementioned practical issue, is removed in CR CgLp.

The superiority of CgLp control structures over other reset control strategies in precision motion control has been shown in many researches [9, 13, 18]. In the remainder of this paper, for the sake of conciseness, only CR CgLp architecture 205 will be studied. However, the same approach can be used for other reset control structures.

For the case of CR CgLp, the magnitude of higher-order harmonics for fre-

frequencies lower than ω_c (where it matters the most for tracking and disturbance rejection [12, 18]) is also affected by parameters other than ω_l . These parameters are ω_r and γ . However, unlike ω_l , these two parameters also affect the DF phase and consequently the amount phase lead created by CR CgLp. This creates a trade-off between reduction of higher-order harmonics magnitude and maximum achievable Phase Advantage (PA) of CR CgLp. Fig. 6 illustrates the trade-off. CgLp will be logically designed to provide phase lead at cross-over frequency, i.e., ω_c . As ω_r approaches ω_c the integral of 3rd harmonic magnitude over frequencies below ω_c decreases significantly. The reduction of integral value is an indication of the reduction of magnitude of higher-order harmonics in general. Furthermore, the peak of higher-order harmonics will also shift to higher frequencies when ω_r approaches higher frequencies. Thus it seems logical to have this peak in frequencies where tracking and disturbance rejection performance is not a matter of concern, i.e., the frequencies after the bandwidth. When ω_r is in $[\omega_c, 1.5\omega_c]$, higher-order harmonics are very low and still a PA up to 35° is achievable. This can be a general guideline for tuning ω_r in CR CgLp.

5. Closed-Loop Transient Response Properties of the CR CgLp Architecture

In the researches done on CgLp control systems in the literature, the only considered design parameter for changing the transient response of systems is phase margin. In the context of linear control systems, phase margin is determining parameter; however, that is not the case for reset control system and especially for the CR architecture presented in this paper. Referring to Eq. (8), speaking in terms of the closed loop, in CR architecture, the reset condition is not only based on the error signal but a linear combination of error and its derivative. This will change transient response of the system as well [38, 22, 20]. In order to study the effect of parameters of CR architecture on transient response of a closed-loop precision motion control system, a data-based approach

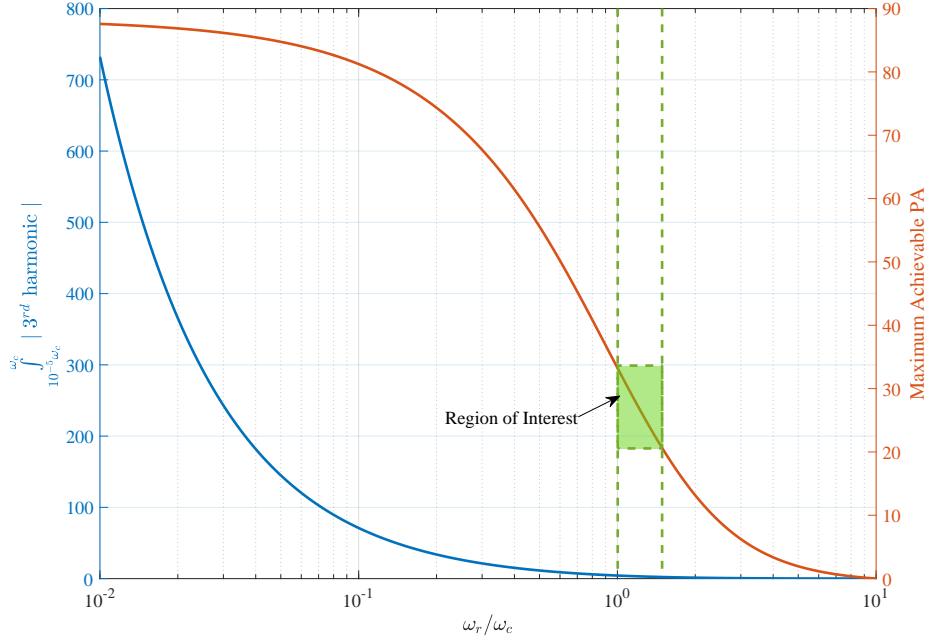


Figure 6: Integral of 3rd harmonic magnitude for frequencies below ω_c and the maximum achievable PA at ω_c vs. the ratio of ω_r to ω_c . $\gamma = -1$.

has been used in this paper.

Fig. 7 shows the block diagram of the control loop. As it is shown in the figure, the reset part of CgLp, i.e., \sum_R , is surrounded by $L(s)$ and $R(s)$ to create a CR CgLp.

Following the discussion in Section 2.1, the plant which is used for this data-based study is a mass system, i.e., $P(s) = 1/s^2$. In experimental validation, it will be shown that the analysis will also hold mass-spring-damper systems.

The H_β condition for stability of the reset control systems necessarily requires the BLS to be stable. Thus, a PID controller is present in the loop. However, according to loop-shaping technique, to ensure the maximum steady-state precision performance for the system, the differentiation part of the PID should be as weak as possible to only guarantee the stability of the BLS. Normally, such a tuning for PID control system will perform poorly in terms transient response in absence of CR CgLp. Nevertheless, it will be shown that the presence CR

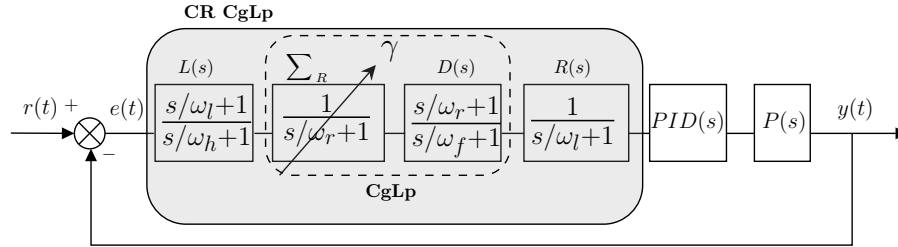


Figure 7: The control loop used for precision motion control using CR CgLp. $P(s)$ is the plant. $PID(s) = k_p (1 + \omega_i/s) \left(\frac{s/\omega_d + 1}{s/\omega_t + 1} \right)$.

CgLp will significantly improve transient response without affecting the maximally precise steady-state performance of the system. In this study, using a rule of thumb, the PID is tuned such that the BLS has 5° phase margin, which is enough to stabilize the BLS and since it has a weak differentiator, does not jeopardize the steady-state precision. The following equation shows the parameters chosen in this regard.

$$\omega_i = \omega_c/10, \quad \omega_d = \omega_c/1.2, \quad \omega_t = 1.2\omega_c \quad (23)$$

And consequently, k_p can be determined according to ω_c . According to the discussions in Section 4, without loss of generality, for this data-based study,

$$\omega_r = 1.2\omega_c. \quad (24)$$

This leaves the effect of γ and ω_l to be studied. Since ω_r and the parameters of PID are fixed, the only parameter which affects the phase margin of the designed system is γ . It has to be noted, that according to Proposition 1, CR
 230 architecture does not change the DF, thus ω_l does not have an effect on phase margin. Fig. 8 shows the open-loop DF of the system under study and also the effect of γ on phase margin. $\gamma = 1$ indicates the base linear system and as the value γ decreases the phase margin will increase. At $\omega = \omega_c$, it can be seen that CR CgLp not only does not change the gain behaviour, but also creates a
 235 positive slope in phase, which resembles the complex-order controllers. In the following, the effect of phase margin and ω_l on overshoot and settling time of

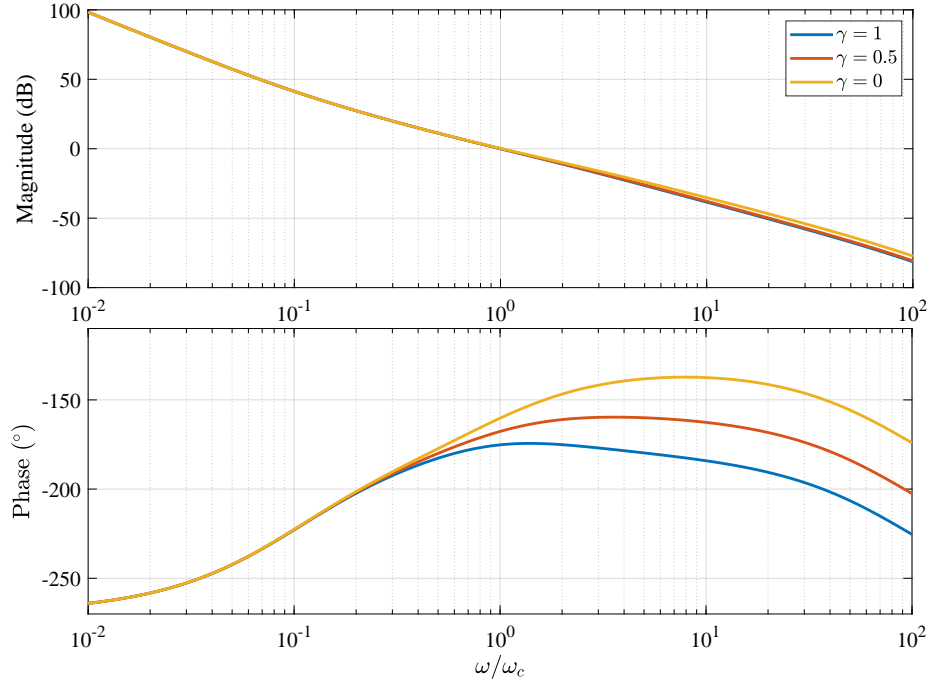


Figure 8: DF of the open loop system for different γ values versus the ration of ω/ω_c .

the closed-loop system will be shown.

5.1. Overshoot

As mentioned before, it is expected that the variation of phase margin caused by variation of γ and the variation on ω_l create different transient responses for the closed-loop system. In order to do a data-based study, a unit step reference was given to the closed-loop system and the the response was simulated using Simulink environment of Matlab. The overshoot versus the variation of ω_l and phase margin is depicted in Fig. 9.

From Fig. 9, it can be concluded that similar to linear controllers, with increase of the phase margin the overshoot decreases almost linearly. Furthermore, for a constant value of phase margin as ω_l decrease the overshoot decreases and for some configurations a non-overshoot performance is realizable. It should be also noted that as ω_l increases, it weakens the lead element $L(s)$ and thus system

gradually tends to the performance of the conventional CgLp. Overshoot of the system in the absence of CR CgLp, i.e., BLS, is 96%.

In the range of Phase Margin (PM) $\in [10, 30]$ and $\omega_l/\omega_c \in [0.1, 1]$, the decrease of overshoot (OS) is almost linear with respect decrease of $\log(\omega_l)$. A fitting operation reveals the following relation between the OS and PM and ω_l .

$$OS = 0.95 \log\left(\frac{\omega_l}{\omega_c}\right) - 0.04PM + 1.25 \quad (25)$$

where PM is in degrees.

240 In order to better illustrate the effect of these two parameters on overshoot and in general transient response of the closed-loop system, one can refer to Fig. 10. For this simulation $\omega_c = 100$ rad/s. Fig. 10a shows the reduction of overshoot by reduction of ω_l , the non-overshoot response is shown to be realizable. However, too much reduction of ω_l can result in long settling times as is the case for
 245 $\omega_l = 10$ rad/s. Obviously, since CgLp does not contain ω_l , it has only one response.

Fig. 10b demonstrates the effect of PM on step response of the system while $\omega_l = 33$ rad/s, the presence of CR architecture amplifies the reduction of overshoot caused by increase of PM. It has to be noted that various values of PM is
 250 achieved by changing γ .

The study shows the significant improve in transient response by CR CgLp. It worth mentioning that it will be showed later that this improvement in transient will not sacrifice the steady-state response.

255 5.2. Settling time

According to Fig. 9 and 10a, reduction of ω_l generally decreases overshoot, it may have an adverse effect on settling time. In order to find a sweet spot where overshoot and settling time are improved simultaneously the same sweep as Fig. 9 has been done for settling time and depicted in Fig. 11. According to
 260 this figure, for a constant ω_l the settling time decreases with increase of PM as like the case for linear controllers. However, there is no linear relation for

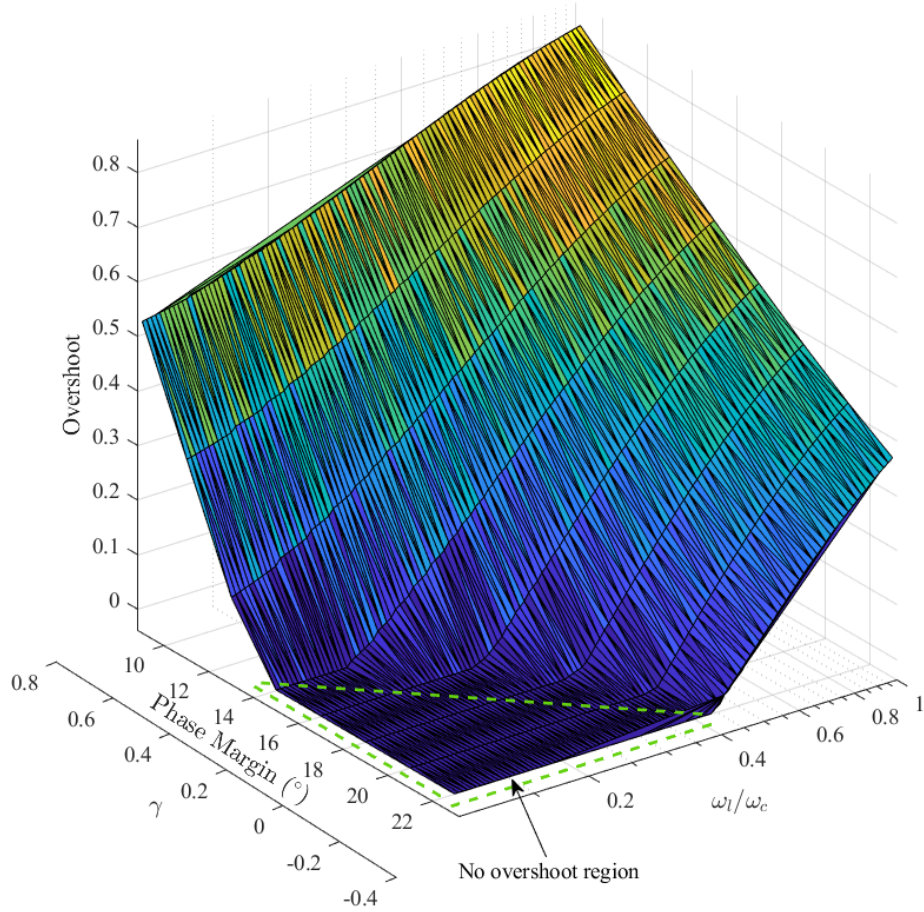
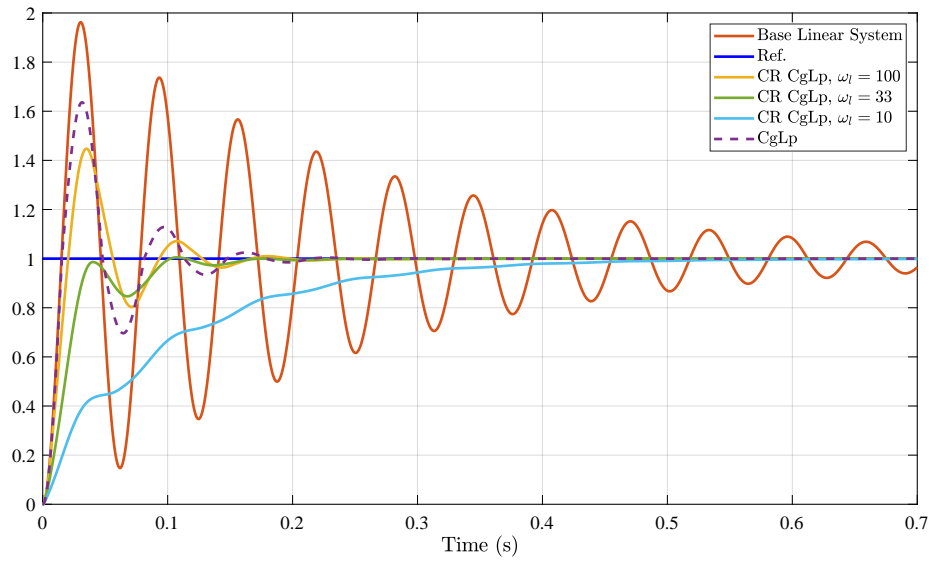


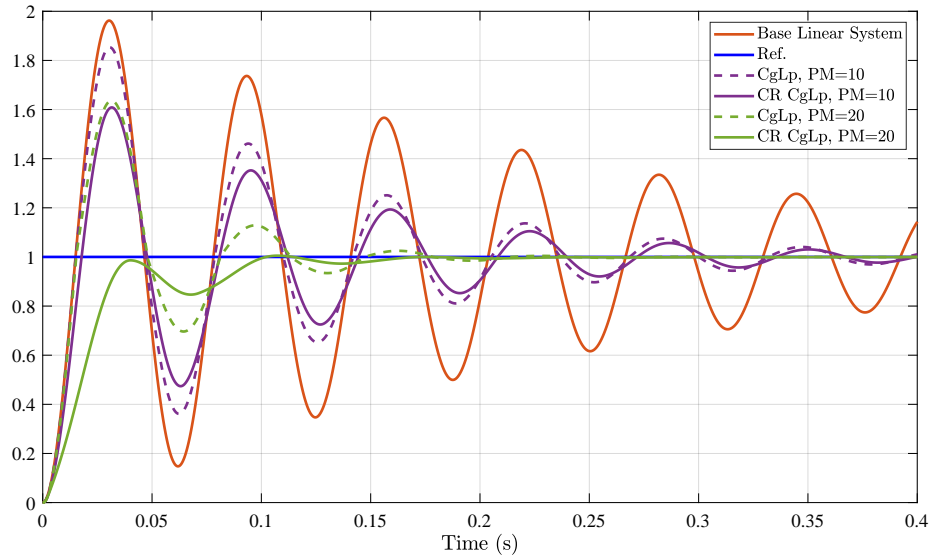
Figure 9: The overshoot of the system to a unit step for phase margin in range of $[5, 22]$ and $\omega_l/\omega_c \in [0.1, 1]$. 5° of the phase margin is provided through base linear system. The overshoot in the absence of the CR CgLp, i.e., BLS, is 0.962.

ω_l/ω_c and settling time.

As a rule of thumb, $\omega_l/\omega_c \in [0.3, 0.6]$ and PM larger than 20° shows a favorable settling time. In this range the settling time of the CR CgLp is shorter than
 265 CgLp and referring to Fig. 9, non-overshoot performance can also be achieved. Thus one can use this general rule of thumb as the tuning guideline of CR CgLp.



(a) Step response of closed-loop system for base linear system, CgLp and CR CgLp for various values of ω_l in rad/s. PM is fixed at 20° and $\omega_c = 100$ rad/s.



(b) Step response of closed-loop system for base linear system, CgLp and CR CgLp for various values of PM. $\omega_c = 33$ rad/s and $\omega_c = 100$ rad/s.

Figure 10: Step response of closed-loop system for base linear system, CgLp and CR CgLp for various values of PM and ω_l .

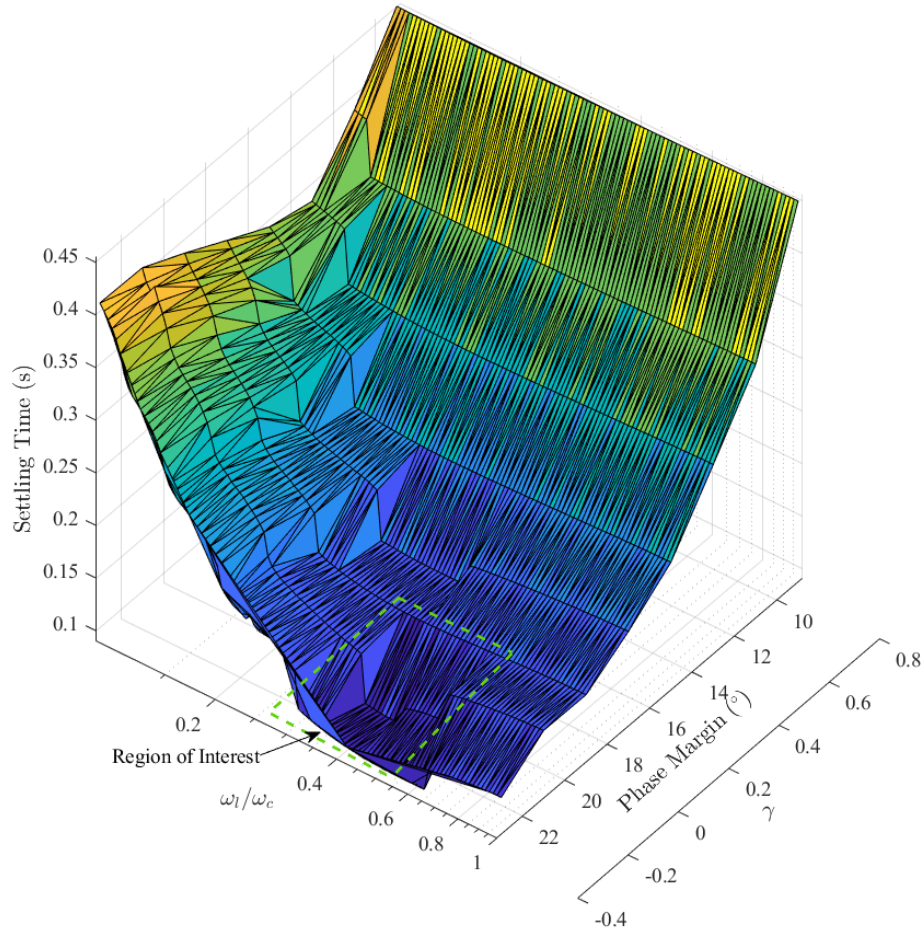


Figure 11: The settling time of the system for a unit step for phase margin in range of $[5, 22]$ and $\omega_1/\omega_c \in [0.1, 1]$. $\omega_c = 100$ rad/s. The settling time in the absence of the CR CgLp, i.e., BLS, is 0.945 s.

6. Closed-Loop Steady-State Performance of the CR CgLp Architecture

270 As discussed earlier, the DF method can be used as an approximation for open-loop steady-state performance of reset control systems. The DF can also be used to find the sensitivity functions of closed-loop reset control systems using the linear relations between open-loop transfer functions and closed-loop sensitivity functions. While the resulted sensitivity plots show the ideal steady-state

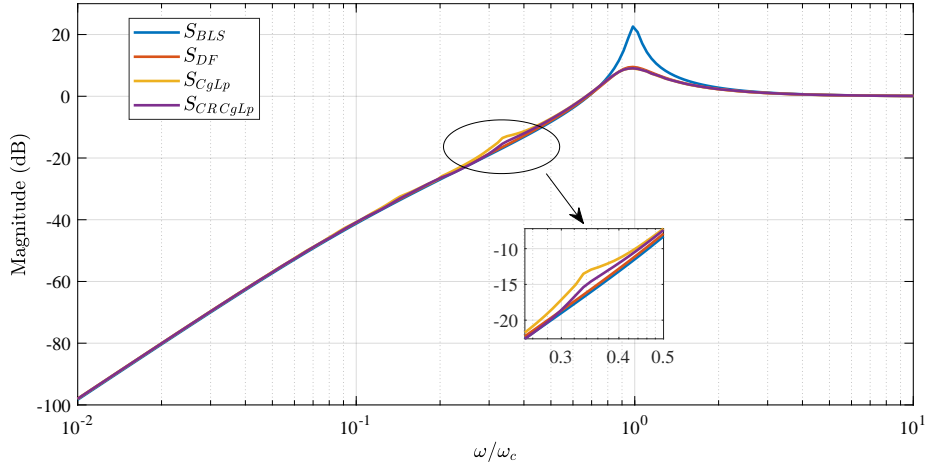


Figure 12: Sensitivity plot for BLS (S_{BLS}) along sensitivity for reset control systems calculated based on DF (S_{DF}), and sensitivity calculated based on infinity norm, i.e., $\frac{\|e(t)\|_2}{\|r(t)\|_2}$ for CgLp and CR CgLp (S_{CgLp} and $S_{CR CgLp}$).

275 behaviour for the designed reset controllers, the presence of higher-order har-
 monics makes achieving it impossible. Thus, as discussed in Section 4, reducing
 higher-order harmonics brings the reset controller closer to the ideal behaviour.
 It is shown that CR architecture and its tuning guidelines can reduce the mag-
 nitude of higher-order harmonics. Thus, it is expected that actual closed-loop
 280 steady-state performance is very close to approximation created by DF. In order
 to verify the latter, a comparison has been made. A series of simulations has
 been run to determine the actual sensitivity functions values for different fre-
 quencies. However, because of nonlinearity of the system, the output will not
 be sinusoidal. To approximate, the second norm of the signals has been used.

285 According to Fig. 12, the presence of either CgLp or CR CgLp reduces the
 peak of sensitivity significantly, which is logical because both of them increase
 the phase margin of the system. At the same time because ω_r is tuned to re-
 duce the higher-order harmonics, it was expected that sensitivity of CgLp and
 CR CgLp, namely, S_{CgLp} and $S_{CR CgLp}$, closely match the sensitivity of the
 290 BLS and the sensitivity approximated by DF, i.e., S_{BLS} and S_{DF} . However, the
 CR CgLp because of lower higher-order harmonics has closer to ideal behaviour

Table 1: The rule of thumb tuning values for parameters of CR CgLp.

Parameter	ω_r	PM	ω_l	ω_h	ω_f
Value	$[\omega_c, 1.5\omega_c]$	$[15^\circ, 25^\circ]$	$[0.3\omega_c, 0.6\omega_c]$	$20\omega_c$	$20\omega_c$

than CgLp. This analysis indicates that the significant improvement in transient behaviour of the CR CgLp architecture not only has almost no negative effect on steady-state behaviour but also positively affects it by reducing the peak of sensitivity.

To summarize the rule of thumb tuning guideline to CR CgLp elements the suggested values for different parameters are presented in Table 1.

The data-based analysis done in previous sections was for mass plants. However, the concepts and the procedure can be done for generalized for mass-spring-damper plants and the suggested rule of thumb tuning values roughly stands for every mass-spring-damper plant. To verify, in the next section, a practical example CR CgLp will be designed and tested for a precision motion setup which has a mass-spring-damper plant with high-frequency modes.

7. Illustrative Practical Example

In order to validate the results of previous sections in precision motion control, an illustrative practical example is presented in this section. Comparison between different controllers such as PID, PID+CgLp and PID+CR CgLp is presented in this section. For the sake of conciseness, in the rest of the paper, PID+CgLp and PID+CR CgLp are shortly called, CgLp and CR CgLp controllers, respectively.

7.1. Plant

The precision positioning stage “Spyder” is depicted in Fig. 13 is a 3 degrees of freedom planar positioning stage which is used for validation. Since reset

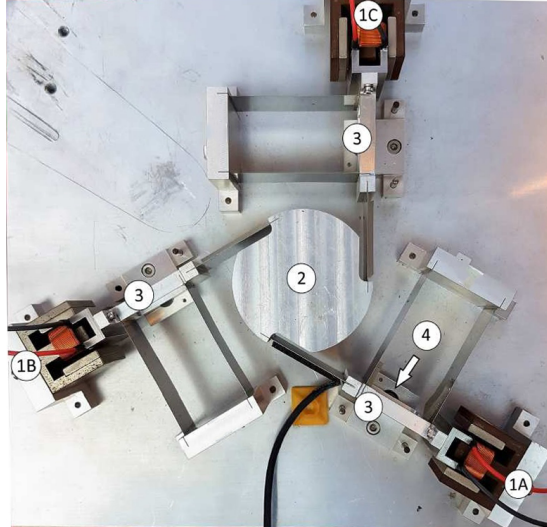


Figure 13: Three degrees of freedom planar precision positioning system called “Spyder”. Spyder is actuated using three voice coil actuators indicated as 1A, 1B and 1C. The actuators are directly connected to masses indicated by 3. Each of these masses are solely connected to the base through two leaf flexures. The position of these masses are being sensed by linear encoders indicated by 4.

controllers in this paper are defined for SISO systems, only the actuator 1A is used to position the mass rigidly connected to it. An NI compactRIO system which is enhanced by a FPGA is used to implement the controllers at a sampling frequency of 10 kHz. Linear current source power amplifier is used to drive the voice coil actuator and a Mercury M2000 linear encoder, indicated as 4 in the Fig. 13 senses the position of the mass with a resolution of 100 nm. The FRF of the stage is identified and depicted in Fig. 14. The identification reveals that the plant shows a behaviour similar to that of a collocated double mass-spring-damper with additional parasitic dynamics at high frequencies. For the sake of better illustration of control design a mass-spring-damper transfer function has been fitted to the FRF data presented in the Eq. (26).

$$P(s) = \frac{9836e^{-0.0001s}}{s^2 + 8.737s + 7376} \quad (26)$$

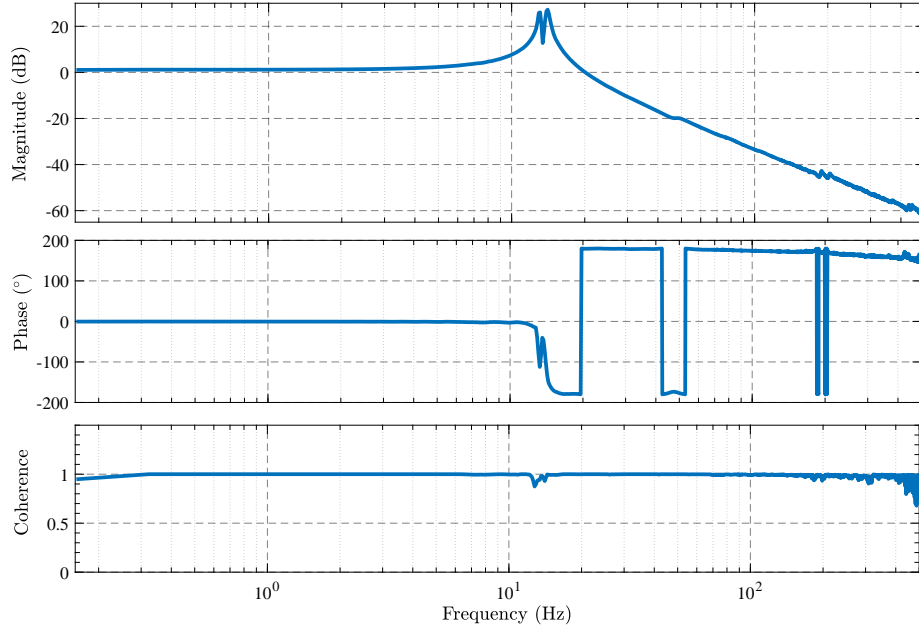


Figure 14: FRF identification of actuator 1A positioning the attached mass.

7.2. Controller Design Approach

315 In order to compare the performance of PID and CR CgLp and show the superiority of the CR CgLp over PID in both steady-state and transient, four controllers were designed. PID controllers are tuned following the tuning rules presented in [26] and reset controllers are designed following the guidelines presented in the paper. The controller loop is already depicted in Fig 7. However, 320 due to presence of noise in practice, a first order low-pass filter, $\frac{1}{s/\omega_z+1}$, has been added to the loop. The parameters for designed controllers is presented in Table 2.

Since the input signal to $L(s)$ is $e(t)$, this element will amplify the noise present in $e(t)$ and thus creates excessive zero crossings and thus excessive reset 325 actions [20]. In order to avoid this phenomenon, ω_h has chosen to be smaller than the rule-of-thumb guidelines provided in previous sections to better attenuate the high-frequency content of the signal. This change in ω_h increases the overshoot in step response, to compensate, ω_l has chosen to be smaller than

Table 2: The parameters for designed controllers. $\omega_c = 400$ Hz.

Parameter	ω_i	ω_d	ω_t	ω_z	ω_r	ω_l	ω_h	ω_f
PID #1	$\omega_c/10$	$\omega_c/2.5$	$2.5\omega_c$	$5\omega_c$	N/A	N/A	N/A	N/A
PID #2	$\omega_c/10$	$\omega_c/5$	$5\omega_c$	$5\omega_c$	N/A	N/A	N/A	N/A
PID #1 + CgLp	$\omega_c/10$	$\omega_c/2.5$	$2.5\omega_c$	$5\omega_c$	ω_c	N/A	N/A	$20\omega_c$
PID #1 + CR CgLp	$\omega_c/10$	$\omega_c/2.5$	$2.5\omega_c$	$5\omega_c$	ω_c	$\omega_c/8$	$5\omega_c$	$20\omega_c$

rule-of-thumb guidelines.

330 PID #1 can also be considered the BLS for the CR CgLp *controller*, since the latter is simply PID #1 with CR CgLp *element* preceding it, as can be seen in Fig. 7. The practical study will show that adding the CR CgLp *element* to a linear PID controller will improve the transient and the steady-state characteristics simultaneously.

335 The open-loop HOSIDF analysis of the CR CgLp controller and the bode plot of the PID controllers are depicted in Fig 15. Due to choosing of ω_r according to Fig. 6 and the architecture of CR CgLp, it can be seen that the magnitude of higher-order harmonics for CR CgLp are at least 60 dB smaller than first-order harmonic. Thus, it is expected that the steady-state response of the system
340 closely follows the amplitude of the first-order harmonic.

7.3. Comparison of the steady-state response

For comparison of the precision of the controllers in terms of steady-state sinusoidal tracking the sensitivity plot of the controllers are depicted in Fig. 15. For this purpose, sinusoidal signals between 1 and 500 Hz has been input as $r(t)$
345 and $\frac{\|e(t)\|_2}{\|r(t)\|_2}$ has been calculated and plotted for each sinusoidal.

In the range of [1, 10] Hz, the sensitivity of all controllers seemed to be lower bounded by -60 dB, this effect is caused by the quantization and the precision of the sensor. However, comparing PID #1 and CR CgLp in range of [10, 500] Hz reveals that performance of the CR CgLp closely matches PID #1 in lower
350 frequencies and its peak of sensitivity is 1.5 dB lower. Thus, one can conclude

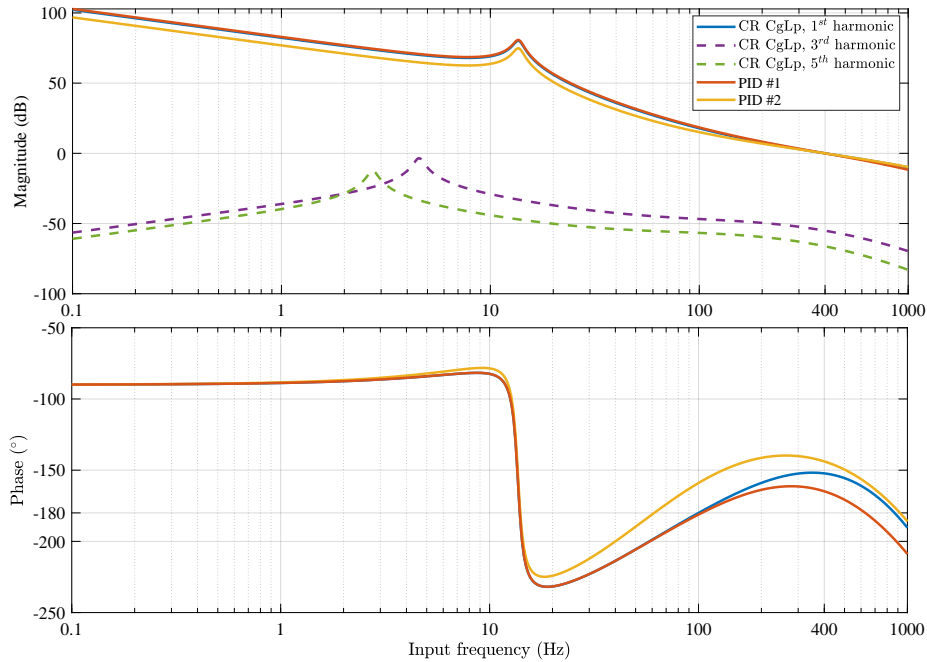


Figure 15: Open-loop HOSIDF analysis of the CR CgLp and Bode plot of PID controllers including the plant. PM for the CR CgLp, PID #1 and PID #2 are respectively, 25° , 15° and 35° .

that the steady-state performance of the linear controller is improved by introducing the proposed element. For the case of PID #2, the clear waterbed effect can be seen, i.e., by widening the band of differentiation, at the cost of losing precision at lower frequencies, the peak of sensitivity is reduced. As opposed by
 355 CR CgLp, where reduction of peak of sensitivity achieved without sacrificing the precision at lower frequencies. Although in linear control context one would expect PID #2 to have better transient response because of lower speak of sensitivity, in the next subsection, it will be shown that this does not hold true in nonlinear context and CR CgLp controller shows better transient response
 360 despite of having higher peak of sensitivity.

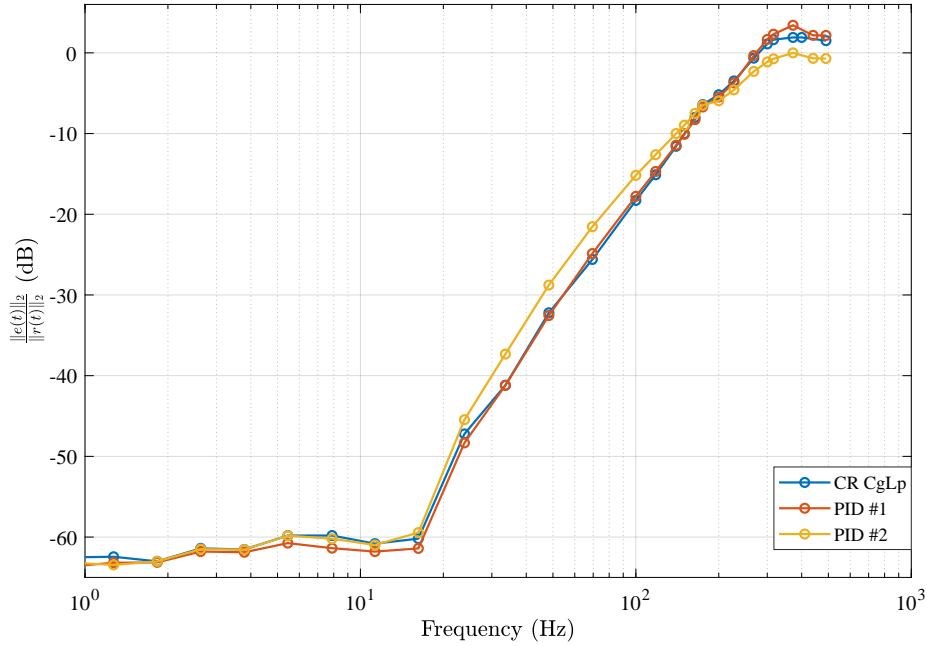


Figure 16: The closed-loop sensitivity of controllers for sinusoidal signals with frequencies in [1, 500] Hz. Frequencies above 500 Hz are not recorded due to the actuator limitations. The sensitivity plot of CgLp closely matches that of CR CgLp, thus, it is not shown for the sake of clarity.

7.4. Comparison of the transient response

For comparison of the step responses of the controllers, a step input of $0.15\mu\text{m}$ height has been used. The response of the controllers are depicted in Fig. 17. As it can be seen the CR CgLp shows a no-overshoot performance where PID #1 shows an overshoot of 38%. It is noteworthy that according to Fig. 16, these two controllers have matching sensitivity at lower frequencies. The settling time has also improved by 25%. This example clearly demonstrates that by adding CR CgLp *element* to an existing PID linear loop, one can achieve a no-overshoot performance and generally significantly improved transient response while maintaining the steady-state precision.

The peak of sensitivity for both CgLp and CR CgLp controllers are the same, however the overshoot of the CR CgLp is 28% lower than CgLp and that of

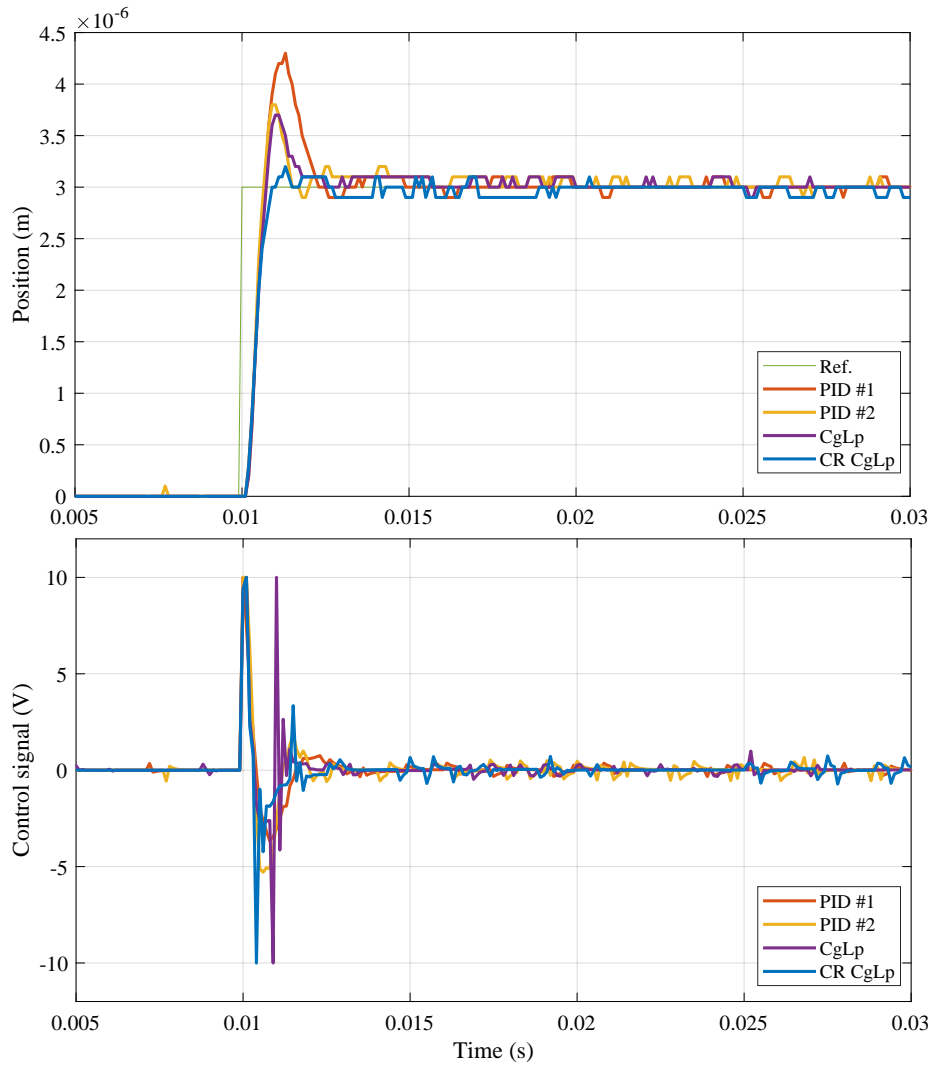


Figure 17: Step response and its corresponding control signal for the controllers introduced in Table 2. The overshoot for CR CgLp, PID #1, PID #2 and CgLp is respectively, 3%, 43%, 28%, 22% and the 96% settling times are respectively, 11.6 ms, 12.2 ms, 14.4 ms and 11.8 ms.

CgLp is 10% lower than that of PID. This results validates that the transient performance of the reset controllers, especially the overshoot, is affected but not solely by PM and peak of sensitivity. The architecture and ω_l also play role. The effect of ω_l will be validated further.

The reduction of overshoot for PID #2 compared to PID #1 was obvious due to wider band of differentiation and thus reduced peak of sensitivity. However, despite the fact that its peak of sensitivity is lower than CR CgLp, the overshoot is still larger than that of CR CgLp. Meanwhile steady-state precision was already shown to be lower than CR CgLp. **It has to be noted, because of the relatively high bandwidth which is chosen for the controllers, i.e., 400 Hz, and limitations of the actuator, control signal for the controllers come close to saturation in only one sample of time. Nevertheless, it will be shown later that this is not the case for lower bandwidths, even for larger references.**

7.5. The effect of ω_l

In Fig. 17, $\omega_l = 50$ Hz. In order to validate the effect of ω_l on transient response, the step response for different values of ω_l while maintaining the other parameters is depicted in Fig. 18. It can be clearly seen that overshoot keeps decreasing with reduction of ω_l/ω_c . Furthermore, it can be also validated that settling time will increase when ω_l/ω_c drops below a certain threshold. This phenomenon can be due to the fact that too much reset and resetting too soon can jeopardize the effect of integrator. It is noteworthy that according to Proposition 1, the value of ω_l does not have an effect on DF and thus steady-state tracking performance of the system.

7.6. Complex-order behaviour

Another interesting behaviour of the CR CgLp controller is the ability to create a complex-order behaviour as depicted in Fig. 19. Two controllers have been designed for $\omega_c = 100$ Hz. In the case of gain variation of 5 dB, ω_c will change to 150 Hz, in such a situation, PID loses 3° of PM while CR CgLp will show a complex-order behaviour, meaning the phase increases while gain decreases [8], and gain 5° more PM. Thus the modulus margin for PID is expected to be decreased and for CR CgLp to be increased.

Furthermore, an increase on overshoot of PID and a decrease in that of CR CgLp is expected. The validation of this expectation has been done in practice

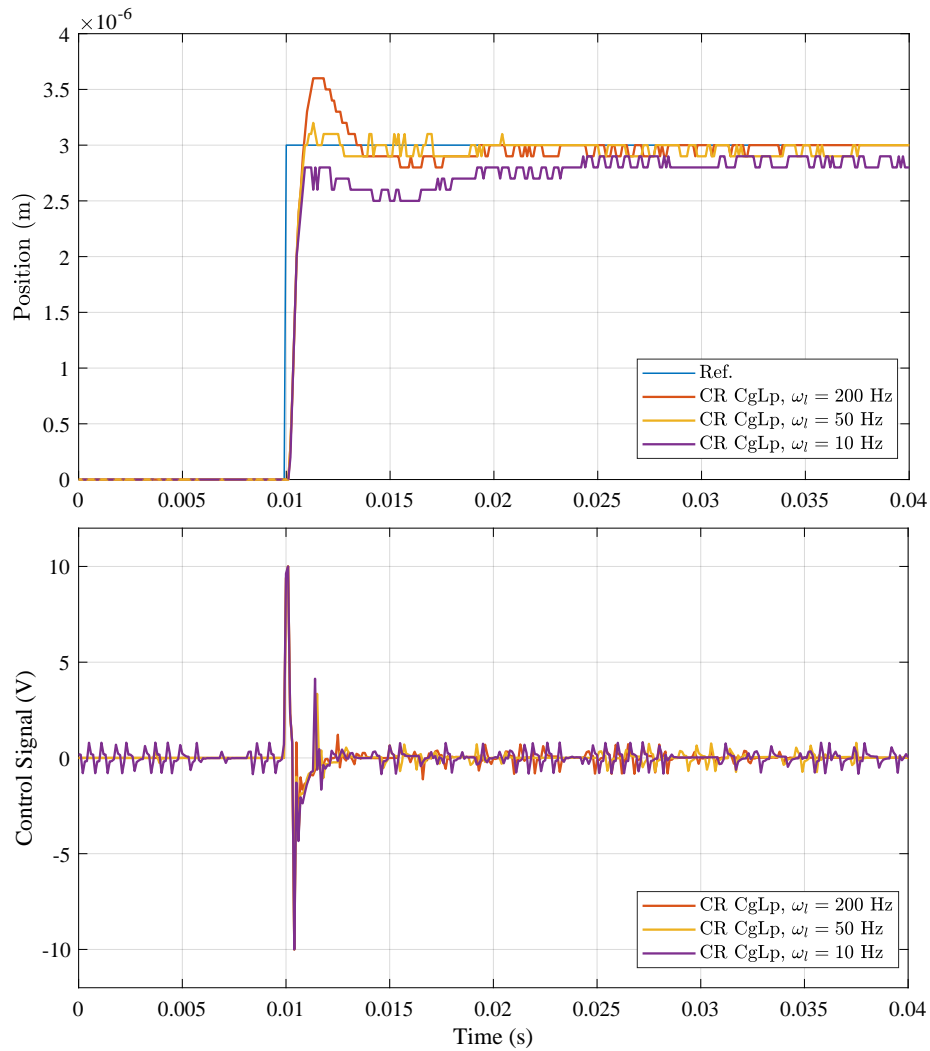


Figure 18: The effect of varying ω_l on transient response and its corresponding control signal of the CR CgLp.

and the step responses are shown in Fig 20. However, the increase in PM is not the only reason for decrease of overshoot in CR CgLp. Since ω_c is increased and ω_l has been kept constant, the ratio of ω_l/ω_c is subsequently reduced, which also helps the reduction of overshoot.

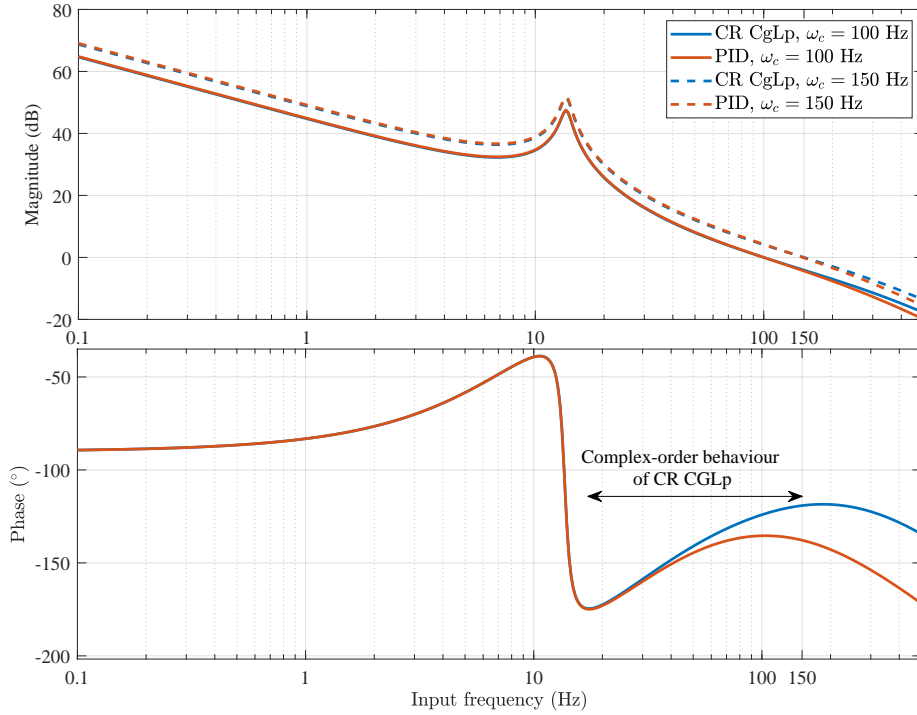


Figure 19: Bode diagram for a PID and DF diagram of a CR CgLp, showing the complex-order behaviour of CR CgLp. PM for CR CgLp at 100 Hz is 55° and for 150 Hz is 60° . PM for the PID at 100 Hz is 45° and for 150 Hz is 43° .

410 8. Conclusion

A new architecture for reset elements, named “Continuous Reset Element” was presented in this paper. Such an architecture consists of having a linear lead and lag element, before and after of a reset element. It was shown that such an architecture not only does not influence the DF gain and phase of re-

415 set elements, but also reduces the magnitude of higher-order harmonics, which will positively effect the steady-state tracking precision of the reset controllers. Furthermore, it was shown that having a strictly proper lag element after the reset element will make the output of the reset element continuous as opposed to conventional reset elements.

420 Moreover, it was shown that such CR architecture also can significantly improve

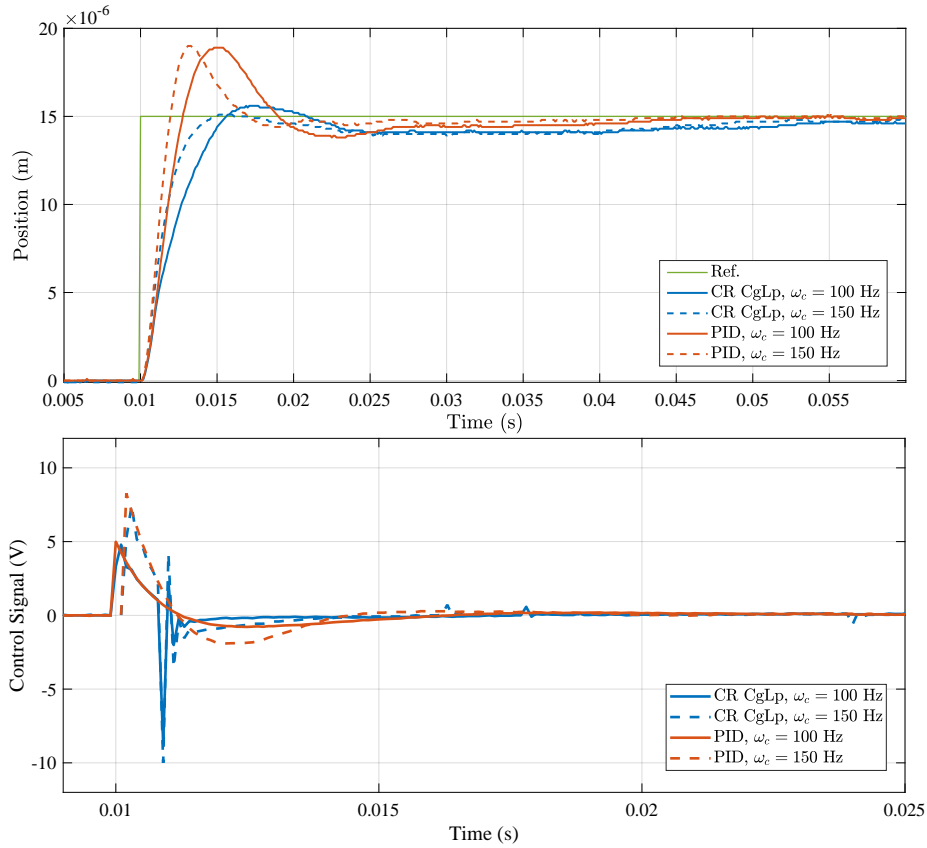


Figure 20: The step response and its corresponding control signal for the controllers shown in Fig. 19 for gain variation of 5 dB. PM for PID increases from 25% to 26% for increased ω_c while PM for CR CgLp decreases from 4% to 0%.

the transient response of the reset control systems for mass-spring-damper plants without negatively affecting the steady-state performance, an overcoming overwaterbed effect. To this end, a numerical study was done on a reset element called CgLp and a mass plant and it was shown that by using the CR architecture, the settling time and overshoot of the CR CgLp control system can be improved both comparing to CgLp element itself and the BLS.

To further validate the achieved results, a practical example was introduced where a precision motion setup was identified and four controllers were implemented and compared in terms of transient and steady-state performance. It

430 was shown that for a mass-spring-damper plant the CR CgLP controller was
able to achieve a no-overshoot performance and a reduced settling time while
matching the steady-state performance of the PID BLS at lower frequencies and
a showing a reduced peak of sensitivity.

However, the presence of a lead element before a reset element can introduce
435 excessive reset actions to the control because of noise. To avoid such a phe-
nomenon a low-pass filter or in general term a shaping filter can be used to
remove the high-frequency content of the signal. For which a more extensive
research is required. The latter can be ongoing work of the propose design.

Acknowledgment

440 This work was supported by NWO, through OTP TTW project #16335.

References

- [1] H. W. Bode, et al., Network analysis and feedback amplifier design.
- [2] J. Clegg, A nonlinear integrator for servomechanisms, Transactions of the
American Institute of Electrical Engineers, Part II: Applications and In-
445 dustry 77 (1) (1958) 41–42.
- [3] I. Horowitz, P. Rosenbaum, Non-linear design for cost of feedback reduc-
tion in systems with large parameter uncertainty, International Journal of
Control 21 (6) (1975) 977–1001.
- [4] K. Krishnan, I. Horowitz, Synthesis of a non-linear feedback system with
450 significant plant-ignorance for prescribed system tolerances, International
Journal of Control 19 (4) (1974) 689–706.
- [5] L. Hazeleger, M. Heertjes, H. Nijmeijer, Second-order reset elements for
stage control design, in: 2016 American Control Conference (ACC), IEEE,
2016, pp. 2643–2648.

- 455 [6] A. Baños, A. Vidal, Definition and tuning of a PI+ CI reset controller, in: 2007 European Control Conference (ECC), IEEE, 2007, pp. 4792–4798.
- [7] O. Beker, C. Hollot, Y. Chait, H. Han, Fundamental properties of reset control systems, *Automatica* 40 (6) (2004) 905–915.
- [8] D. Valério, N. Saikumar, A. A. Dastjerdi, N. Karbasizadeh, S. H. Hossein-Nia, Reset control approximates complex order transfer functions, *Nonlinear Dynamics* 97 (4) (2019) 2323–2337.
- 460 [9] N. Saikumar, R. K. Sinha, S. H. HosseinNia, “constant in gain lead in phase” element– application in precision motion control, *IEEE/ASME Transactions on Mechatronics* 24 (3) (2019) 1176–1185.
- 465 [10] A. Bisoffi, R. Beerens, W. Heemels, H. Nijmeijer, N. van de Wouw, L. Zaccarian, To stick or to slip: A reset PID control perspective on positioning systems with friction, *Annual Reviews in Control* 49 (2020) 37–63. doi:<https://doi.org/10.1016/j.arcontrol.2020.04.010>.
URL <https://www.sciencedirect.com/science/article/pii/S1367578820300201>
- 470 [11] A. Baños, A. Barreiro, *Reset control systems*, Springer Science & Business Media, 2011.
- [12] N. Karbasizadeh, A. A. Dastjerdi, N. Saikumar, D. Valério, S. H. Hossein Nia, Benefiting from linear behaviour of a nonlinear reset-based element at certain frequencies, in: 2020 Australian and New Zealand Control Conference (ANZCC), 2020, pp. 226–231. doi:[10.1109/ANZCC50923.2020.9318363](https://doi.org/10.1109/ANZCC50923.2020.9318363).
- 475 [13] A. A. Dastjerdi, S. H. Hosseinnia, A frequency-domain tuning method for a class of reset control systems, *IEEE Access* 9 (2021) 40950–40962.
- 480 [14] D. Nesic, A. R. Teel, L. Zaccarian, Stability and performance of siso control systems with first-order reset elements, *IEEE Transactions on Automatic Control* 56 (11) (2011) 2567–2582. doi:[10.1109/TAC.2011.2114436](https://doi.org/10.1109/TAC.2011.2114436).

- [15] D. Wu, G. Guo, Y. Wang, Reset integral-derivative control for hdd servo systems, *IEEE Transactions on Control Systems Technology* 15 (1) (2006) 161–167.
- 485
- [16] Y. Zheng, Y. Chait, C. Hollot, M. Steinbuch, M. Norg, Experimental demonstration of reset control design, *Control Engineering Practice* 8 (2) (2000) 113–120.
- [17] Q. Chen, Y. Chait, C. Hollot, Analysis of reset control systems consisting of a fore and second-order loop, *J. Dyn. Sys., Meas., Control* 123 (2) (2001) 279–283.
- 490
- [18] N. Karbasizadeh, N. Saikumar, S. Hossein Nia Kani, Fractional-order single state reset element, *Nonlinear Dynamics* 104 (1) (2021) 413–427. doi: 10.1007/s11071-020-06138-9.
- [19] Y. Guo, Y. Wang, L. Xie, H. Li, W. Gui, Optimal reset law design and its application to transient response improvement of hdd systems, *IEEE Transactions on Control Systems Technology* 19 (5) (2011) 1160–1167. doi: 10.1109/TCST.2010.2059027.
- 495
- [20] C. Cai, A. A. Dastjerdi, N. Saikumar, S. HosseinNia, The optimal sequence for reset controllers, in: *2020 European Control Conference (ECC)*, 2020, pp. 1826–1833. doi:10.23919/ECC51009.2020.9143690.
- 500
- [21] G. Zhao, D. Nešić, Y. Tan, C. Hua, Overcoming overshoot performance limitations of linear systems with reset control, *Automatica* 101 (2019) 27–35. doi:<https://doi.org/10.1016/j.automatica.2018.11.038>.
URL <https://www.sciencedirect.com/science/article/pii/S0005109818305727>
- 505
- [22] S. J. A. M. van den Eijnden, M. F. Heertjes, W. P. M. H. Heemels, H. Nijmeijer, Hybrid integrator-gain systems: A remedy for overshoot limitations in linear control?, *IEEE Control Systems Letters* 4 (4) (2020) 1042–1047. doi:10.1109/LCSYS.2020.2998946.
- 510

- [23] A. R. Teel, Continuous-time implementation of reset control systems, *Trends in Nonlinear and Adaptive Control* (2022) 27–41.
- [24] J. H. Le, A. R. Teel, Passive soft-reset controllers for nonlinear systems, arXiv preprint arXiv:2104.11414.
- 515 [25] F. Boeren, T. Oomen, M. Steinbuch, Iterative motion feedforward tuning: A data-driven approach based on instrumental variable identification, *Control Engineering Practice* 37 (2015) 11–19.
- [26] R. M. Schmidt, G. Schitter, A. Rankers, The design of high performance mechatronics-: high-Tech functionality by multidisciplinary system integration, IOS Press, 2020.
- 520 [27] S. van den Eijnden, M. Heertjes, H. Nijmeijer, Robust stability and nonlinear loop-shaping design for hybrid integrator-gain-based control systems, in: *2019 American Control Conference (ACC)*, 2019, pp. 3063–3068. doi:10.23919/ACC.2019.8814888.
- 525 [28] D. J. Rijlaarsdam, V. Van Geffen, P. Nuij, J. Schoukens, M. Steinbuch, Frequency domain based feed forward tuning for friction compensation, *Proc. ASPE spring TM* (2010) 129–134.
- [29] Y. Guo, L. Xie, Y. Wang, *Analysis and Design of Reset Control Systems*, Institution of Engineering and Technology, 2015.
- 530 [30] S. Polenkova, J. W. Polderman, R. Langerak, Stability of reset systems, in: *Proceedings of the 20th International Symposium on Mathematical Theory of Networks and Systems*, 2012, pp. 9–13.
- [31] D. Nešić, L. Zaccarian, A. R. Teel, Stability properties of reset systems, *Automatica* 44 (8) (2008) 2019–2026.
- 535 [32] P. Vettori, J. W. Polderman, R. Langerak, A geometric approach to stability of linear reset systems, in: *21st International Symposium on Mathematical Theory of Networks and Systems, MTNS 2014*, University of Groningen, 2014, pp. 776–783.

- [33] C. Prieur, I. Queinnec, S. Tarbouriech, L. Zaccarian, Analysis and synthesis
540 of reset control systems, *Foundations and Trends in Systems and Control*
6 (2-3) (2018) 117–338.
- [34] A. A. Dastjerdi, A. Astolfi, S. H. HosseinNia, Frequency domain stability
method for reset systems (2021). [arXiv:2009.00569](https://arxiv.org/abs/2009.00569).
- [35] Y. Guo, Y. Wang, L. Xie, Frequency-domain properties of reset systems
545 with application in hard-disk-drive systems, *IEEE Transactions on Control
Systems Technology* 17 (6) (2009) 1446–1453.
- [36] P. Nuij, O. Bosgra, M. Steinbuch, Higher-order sinusoidal input describing
functions for the analysis of non-linear systems with harmonic responses,
Mechanical Systems and Signal Processing 20 (8) (2006) 1883–1904.
- 550 [37] N. Saikumar, K. Heinen, S. H. HosseinNia, Loop-shaping for reset control
systems: A higher-order sinusoidal-input describing functions approach,
Control Engineering Practice 111 (2021) 104808.
- [38] A. A. Dastjerdi, S. H. Hosseinnia, A frequency-domain tuning method for
a class of reset control systems, *IEEE Access* 9 (2021) 40950–40962. doi:
555 10.1109/ACCESS.2021.3064812.